

# Coordinate transformation based design of confined metamaterial structures

Borislav Vasić,<sup>1,\*</sup> Goran Isić,<sup>2,1</sup> Radoš Gajić,<sup>1</sup> and Kurt Hingerl<sup>3</sup>

*<sup>1</sup>Institute of Physics, Pregrevica 118,*

*P. O. Box 68, 11080 Belgrade, Serbia*

*<sup>2</sup>School of Electronic and Electrical Engineering,*

*University of Leeds, Leeds LS2 9JT, United Kingdom*

*<sup>3</sup>Christian Doppler Lab, Institute for Semiconductor and Solid State Physics,*

*University of Linz, A-4040 Linz, Austria*

## Abstract

The coordinate transformation method (CTM) is a powerful tool that exploits the duality between matter and geometry. Several CTM approaches for design of electromagnetic metamaterial devices have been developed so far. In most applications, electromagnetic fields are well confined in two-or three dimensions and may be imagined as being within spatial domains defined by perfectly conducting boundaries (PCBs). We show that PCBs are invariant under the change of geometry introduced by the presence of transformation media and give a formulation of CTM for such confined structures. The range of applications of a design strategy based on confined structures is shown to go well beyond structures that are coated with metallic layers. Electromagnetic beams that propagate in free space are already confined. In that case, we use PCBs as a scaffolding and remove them after the device has been designed. A beam rotator, a two-dimensional analogue of an imperfect electromagnetic wormhole and an arbitrary complex structure are designed by the proposed method and validated by single-frequency finite element method simulations.

## INTRODUCTION

The duality between spatial geometry (or space-time geometry, in general [1]) and material parameters in macroscopic electromagnetism [2] has been recognized with the development of general covariance of Maxwell equations. The procedure by which an arbitrary geometry is mapped to material parameters is called the coordinate transformation method (CTM) and the material with modified parameters the transformation media [3], [4].

Various forms of CTM have fruitfully been exploited for a diversity of computational problems: designing perfectly matched layers (PMLs) for simulating open boundaries in finite-difference time-domain and finite element methods (FEM) [5], [6], [7], simplifying the geometry of complex computational domains [8], representing waveguide bends and twists by equivalent straight segments [9], [10] and formulating novel perturbation schemes for anisotropic materials [11]. Transformation media have first been regarded as merely fictional anisotropic materials having real (for real-space transformations) or complex (for complex coordinate transformations [6],[12], as in the case of PMLs) parameters as an aid for numerical modeling. This changed in the course of time since transformation media could be implemented as a metamaterial [3] and CTM used to design structures that fabricate arbitrary geometries for the electromagnetic fields.

Already there exist several distinct strategies for the CTM-based design of metamaterial structures. A continuous transformation of the whole space,  $\mathbb{R}^3$ , gives devices that are inherently invisible (like invisibility cloaks [3], electromagnetic field concentrators [13], rotators [14] and perfect lenses [15], [1]). In [1] CTM has been applied to space-time in order to design devices where such elusive effects as the optical Aharonov-Bohm effect or black holes could be observed. CTM has also been used to design metamaterial devices that implement a virtual electromagnetic three-manifold with a wormhole in it [16]. Most recently, the embedded coordinate transformation technique has been described [17]: a coordinate transformation of a finite domain  $D$ , such that its boundary  $\partial D$  is left invariant, is embedded into the surrounding space  $\mathbb{R}^3 \setminus D$  yielding devices that can affect electromagnetic wave propagation in their exterior (due to the discontinuity of the transformation on  $\partial D$ ).

In this paper, we develop a new design strategy by applying CTM to confined structures where we mean structures enclosed within a perfect electric conductor (PEC) or perfect magnetic conductor (PMC) boundary. It is shown that applying CTM to confined structures

enhances the design freedom compared to above mentioned strategies which all (in one way or another) apply CTM to boundless spaces. Our approach has a broad range of applications due to the fact that in practice electromagnetic fields are always confined in space, like in waveguides, electromagnetic cavities or like an electromagnetic beam propagating in free space. The boundary conditions can be regarded either as a physically imposed condition (as in waveguides with metallic coatings) or merely as an mathematical tool to be used on the boundaries of the domain of interest where the intensity of the fields is negligible. We explain how an arbitrary orthogonal transformation (rotation or translation) of electromagnetic fields may be achieved outside the transformation media.

## THE COORDINATE TRANSFORMATION METHOD AND CONFINED STRUCTURES

The operation of transformation media devices and CTM [3] can be best understood by looking at Fig. 1. The notation and terminology parallels that of Leonhardt and Philbin in [1] and [18]. We focus on PEC conditions, while the same applies to PMC conditions.

Figure 1 (a) shows a domain  $D'$  its PEC boundary  $\partial D'$ , the Cartesian coordinates  $x^{i'}$  and the Euclidean metric  $g_{i'j'} = \delta_{i'j'}$  ( $\delta_{i'j'}$  is the Kronecker delta). Henceforth, all indices run from 1 to 3 and we adopt the Einstein summation convention by which summation over repeated indices is implied. The electric permittivity and magnetic permeability of the medium within  $D'$  are labeled  $\varepsilon^{i'j'}$  and  $\mu^{i'j'}$ , respectively. Domain  $D'$  is referred to as the *electromagnetic domain*.

The *physical domain*  $D$  with its PEC boundary  $\partial D$  shown in Fig. 1 (b) is obtained by the mapping:

$$x^i = x^i(x^{1'}, x^{2'}, x^{3'}), \quad \Lambda_{i'}^i = \frac{\partial x^i}{\partial x^{i'}}, \quad \Lambda_i^{i'} = \frac{\partial x^{i'}}{\partial x^i}. \quad (1)$$

The geometries of  $D'$  and  $D$  are equivalent if the metric in  $D$  is

$$g_{ij} = \Lambda_i^{i'} \Lambda_j^{j'} g_{i'j'}, \quad (2)$$

since in that case  $x^i$  can be regarded as curved coordinates in  $D'$ . This is illustrated by the curved shape of  $D$  and its Cartesian grid in Fig. 1 (b). However, a physical significance may be attributed to this change of coordinates by exploiting the duality between matter and geometry in Maxwell equations. The Maxwell equations have a Cartesian form with respect

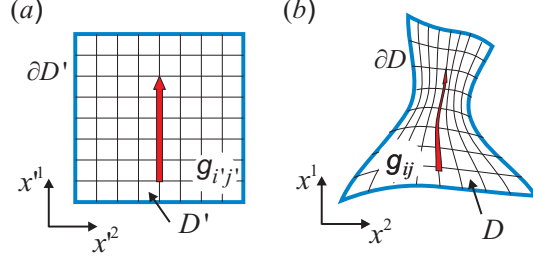


FIG. 1: (Color online) (a) The *electromagnetic domain*  $D'$  with Cartesian coordinates  $x^{i'}$  (b) The *physical domain*  $D$  with Cartesian coordinates  $x^i$ . The non-trivial metric tensor  $g_{ij}$  signifies that the mapping of  $D'$  onto  $D$  may be interpreted as the introduction of curved coordinates  $x^i$  in  $D'$ . The Cartesian grid in (a) is mapped onto a curved grid in (b). Red arrows show that electromagnetic beams propagate along the Cartesian grid in the *electromagnetic domain*. Blue lines stand for  $\partial D'$  and  $\partial D$ , the PEC boundaries.

to  $x^i$  if the change of metrics from  $g_{ij}$  to  $\delta_{ij}$  is mapped to the material parameters as given by [18], [13]

$$\varepsilon^{ij} = \Lambda^{-1} \Lambda_{i'}^i \Lambda_{j'}^j \varepsilon^{i'j'}, \quad \mu^{ij} = \Lambda^{-1} \Lambda_{i'}^i \Lambda_{j'}^j \mu^{i'j'}, \quad (3)$$

where  $\Lambda$  is the determinant of  $\Lambda_{i'}^i$ . Hence,  $x^i$  are regarded as Cartesian coordinates in the *physical domain*  $D$  while the electromagnetic equivalence of  $D$ , filled with transformation media  $\varepsilon^{ij}$  and  $\mu^{ij}$ , with the *electromagnetic domain*  $D'$ , filled with  $\varepsilon^{i'j'}$  and  $\mu^{i'j'}$ , is attained by (3). In other words, if domain  $D$  is filled with a metamaterial with  $\varepsilon^{ij}$  and  $\mu^{ij}$  given by (3), the electromagnetic fields will perceive  $D$  as if  $x^{i'}(x^1, x^2, x^3)$  were the Cartesian coordinates and the medium described by  $\varepsilon^{i'j'}$  and  $\mu^{i'j'}$  (expressed in  $x^{i'}$ ). This is the meaning of the curved grid in  $D$ . The described CTM procedure is valid irrespective of the medium in  $D'$ , but the principle can be best explained by assuming that it is homogeneous. According to the Fermat's principle (see Ref. [18]), electromagnetic beams in a homogeneous medium propagate along the shortest path which is a straight line in Cartesian coordinates. This is indicated by the red arrow in Fig. 1 (a). The corresponding red arrow in Fig. 1 (b) is curved because the transformation media make the beam perceive  $x^i$  as curved coordinates. A similar reasoning shows that transformation media enable the control of field distribution, as shown schematically in Fig. 1 (b) where the arrow width changes to follow the change in spacing between adjacent coordinate lines  $x^{i'}$ .

The electric and magnetic fields in  $D'$  are given by  $E_{i'}$  and  $H_{i'}$ , so the transformed fields

in  $D$  are

$$E_i = \Lambda_i^{i'} E_{i'}, \quad H_i = \Lambda_i^{i'} H_{i'}, \quad (4)$$

hence by choosing appropriate  $\Lambda_i^{i'}$ , the field polarization can be controlled as well.

To prove that the PEC conditions on  $\partial D'$  are consistent with PEC conditions on  $\partial D$ , consider a point  $P'$  on  $\partial D'$  and two vectors,  $d\mathbf{u}' = du^{i'} \mathbf{e}_{i'}$  and  $d\mathbf{v}' = dv^{i'} \mathbf{e}_{i'}$  in its vicinity defining a surface element  $d^2\mathbf{S}' = d\mathbf{u}' \times d\mathbf{v}'$  on  $\partial D'$ . Let the electric field,  $\mathbf{E}'$ , in the vicinity of  $P'$  be described by its covariant coordinates,  $E_{i'}$ . The PEC boundary conditions read

$$\{\mathbf{E}' \times (d\mathbf{u}' \times d\mathbf{v}')\}^{j'} = E_{i'} \left( du^{i'} du^{j'} - du^{j'} dv^{i'} \right) = 0. \quad (5)$$

Let  $P$  be the point on  $\partial D$  that is the image of  $P'$  and  $d\mathbf{u} = du^i \mathbf{e}_i$ ,  $d\mathbf{v} = dv^i \mathbf{e}_i$  and  $\mathbf{E}$ , with covariant coordinates given by (4), images of  $d\mathbf{u}'$ ,  $d\mathbf{v}'$  and  $\mathbf{E}'$ , respectively. The contravariant coordinates  $du^i$  and  $dv^i$  are given by

$$du^i = \Lambda_{i'}^i du^{i'}, \quad dv^i = \Lambda_{i'}^i dv^{i'}. \quad (6)$$

In expressing the boundary conditions on  $\partial D$ , a care has to be taken about the duality in the interpretation of the metrics in  $D$ , since the dot product "  $\cdot$  " and the cross product "  $\times$  " are defined in terms of the metric tensor. If the metric is taken to be  $g_{ij}$ , the PEC condition on  $\partial D'$  is obtained in the curved coordinates  $x^i$ . If the metric is  $\delta_{ij}$ , corresponding to the Cartesian coordinates  $x^i$  in  $D$ , the boundary conditions applying in the *physical domain* are obtained. Using the identity

$$\mathbf{A} \times (\mathbf{B} \times \mathbf{C}) = \mathbf{B}(\mathbf{A} \cdot \mathbf{C}) - \mathbf{C}(\mathbf{A} \cdot \mathbf{B}), \quad (7)$$

that applies irrespective of the metrics, we obtain

$$\{\mathbf{E} \times (d\mathbf{u} \times d\mathbf{v})\}^j = \Lambda_i^{m'} \Lambda_{k'}^i \Lambda_{l'}^j E_{m'} \left( du^{k'} dv^{l'} - du^{l'} dv^{k'} \right). \quad (8)$$

Since  $\Lambda_i^{m'} \Lambda_{k'}^i = \delta_{k'}^{m'}$ , the right hand side of (8) becomes

$$\{\mathbf{E} \times (d\mathbf{u} \times d\mathbf{v})\}^j = \Lambda_{l'}^j E_{k'} \left( du^{k'} dv^{l'} - du^{l'} dv^{k'} \right) = 0. \quad (9)$$

The above quantity is zero irrespective of the metrics because of (5), proving that the PEC conditions apply in the *physical domain* as well. Replacing  $E_i$  with  $H_i$ , the same can be shown for PMC boundary conditions.

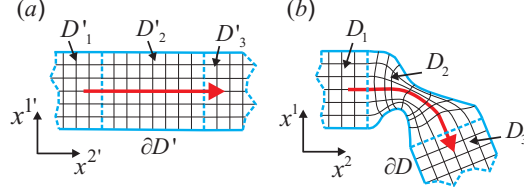


FIG. 2: (Color online) (a) The subdomains in the *electromagnetic domain* (b) their images in the *physical domain*. A distinction is made between subdomains,  $D_1$  and  $D_3$ , that are only rotated or translated and thus require no transformation media. The subdomain  $D'_2$  is mapped to  $D_2$  with a change in shape. Hence, a transformation media needs to be placed inside to implement the curvature of the grid. Dashed lines denote subdomain boundaries, but have no physical significance. Particularly, the left and right dashed-line boundaries of  $D'_1$  and  $D'_3$  mean that  $D'_1$  and  $D'_3$  might extend beyond what is shown in the Figure.

To illustrate the utility of transformation media, the domains  $D'$  and  $D$  are divided into three subdomains,  $D'_1$ ,  $D'_2$ ,  $D'_3$  and  $D_1$ ,  $D_2$ ,  $D_3$ , respectively, as shown in Figs. 2 (a) and (b). The subdomains  $D'_1$ ,  $D'_2$  and  $D'_3$  are mapped to subdomains  $D_1$ ,  $D_2$  and  $D_3$ .  $D_1$  is identically mapped to  $D'_1$ ,  $D'_2$  is distorted and mapped to  $D_2$  so that it continuously connects  $D_1$  and  $D_3$  in Fig. 2 (b) and  $D'_3$  is mapped to  $D_3$  without any distortion but it is displaced or rotated with respect to  $D'_3$ . This implies that the mappings of  $D'_1$  and  $D'_3$  to  $D_1$  and  $D_3$  are orthogonal

$$\Lambda_i^{i'} \Lambda_j^{j'} \delta^{ij} = \delta^{i'j'}, \quad \Lambda = 1. \quad (10)$$

Orthogonal mappings are particularly interesting if the media is isotropic,

$$\varepsilon^{i'j'} = \varepsilon \delta^{i'j'}, \quad \mu^{i'j'} = \mu \delta^{i'j'}, \quad (11)$$

because in that case Eq. (3) asserts that  $\varepsilon^{ij} = \varepsilon \delta^{ij}$  and  $\mu^{ij} = \mu \delta^{ij}$ . Henceforth we assume that (11) is met in  $D'_1$  and  $D'_3$  (simply,  $D'_2$  is defined so that it contains all the anisotropic parts of  $D'$ ) which confines the transformation media to  $D_2$ .

For example [19], if  $D_2$  is designed to yield a bend of an initially straight waveguide structure  $D'$ , a metamaterial needs to be put only in a  $D_2$  shaped domain to guide the waves along the curved grid of  $D$ . A wave that goes through such a metamaterial, will exit and continue with a rotated direction of propagation. Because of the relationship (4) between fields in  $D_3$  and those in  $D'_3$ , it is more appropriate to use the term transformed instead of transmitted for the wave in  $D_3$ . In the next section, we give an example of a device

that rotates free-space electromagnetic beams. Imagine that  $D'_1$  and  $D'_3$  in Fig. 2 (a) extend to infinity on left and right, respectively. For an electromagnetic beam propagating near the central axis of  $D'$  with a width smaller than the width of  $D'$ , the PEC boundaries are merely conceptual. Passing through an annular shaped domain  $D_2$ , the beam will continue to propagate in free space but along a different direction and, in general, with a changed polarization, according to (4).

Using orthogonal mappings for domains  $D_1$  and  $D_3$  continuously attached to the domain  $D_2$  with transformation media, we have established a clear and simple recipe for obtaining transformed fields *outside* the transformation media. This could not be achieved with the CTM strategy that was first proposed in [3]. It includes concentrators [13], rotators [14], metamaterial coatings for reshaping PEC scatterers, [20], and perfect lenses [21], [15]. Though perfect lenses can alter the fields outside the metamaterial, it is only in its immediate vicinity, because the transformation media of a perfect lens implement a multi-valued electromagnetic space, [1], which is unfolded to multiple points in the physical space, see also [15]. A more recent strategy reported in [16] and [22], implements virtual three-manifolds with wormholes using metamaterials. Such structures also affect the field behavior far from the metamaterial device, relying on the change of spatial topology which implies singular material parameters (because the metrics represented in a  $R^3$  coordinate-space needs to be singular).

In [17] a CTM technique based on embedded coordinate transformations has been described. The technique offers the means for changing the fields outside the metamaterial device and was used for designing a beam shifter and a beam splitter. In transferring the fields from transformation media to the exterior, it is required that no reflection occurs. Reference [17] reports a sufficient condition for the device to be reflectionless. It is understood that such a condition is to be met in parts of the interface where the fields are nonzero. Our approach with a continuous transition between subdomains  $D_i$  offers an alternative and perhaps more natural perspective. We emphasize that in it a transformation relationship given by (4) is established for the full length of an electromagnetic beam, and that this inherently means that the devices are reflectionless.

Metamaterial structures designed using CTM enable a redistribution the electromagnetic fields within the metamaterial device. This is achieved in all of the above mentioned devices which employ CTM on a boundless space. Also, Ref. [23] describes how metamaterial

layers can be used in waveguides coated by PEC for creating narrowed-down segments of a waveguide, without causing reflection or phase shifts. In terms of the above discussion, these layers correspond to transformation media that would be filled in a narrowed-down domain  $D_2$ , leaving  $D_1$  and  $D_3$  same as  $D'_1$  and  $D'_3$ .

Compared to existing CTM design concepts, the approach described here is well-suited for developing metamaterial structures that steer confined electromagnetic fields: passing through the device, the wave is displaced or rotated with respect to an arbitrary axis. Its application is not limited to physically confined structures, as explained in detail on the example of a beam rotator in the next section. Additionally, our approach gives a comprehensive overview of how the fields are controlled in confined (bounded) structures, as an arbitrary distortion of  $D'_2$  to  $D_2$  is readily achieved. Perhaps the main application of devices that change the fields only in the metamaterial is in miniaturizing waveguides and electromagnetic cavities, or in changing their shape to satisfy some external constraints. Several authors have previously considered CTM applications for waveguides in, [9], [10], [23] and [19], for both modeling and purposes of designing metamaterial structures, but an extensive formulation of the design strategy has not been reported so far.

## EXAMPLES AND NUMERICAL VALIDATION

Some applications of ideas developed in the previous section to physically confined structures have been discussed recently, [9], [10], [23] and [19]. Therefore, we give examples of structures used for manipulating free-space electromagnetic beams where the PEC boundaries are fictional. Vacuum is assumed as the exterior while the subdomains corresponding to  $D_1$ ,  $D'_1$ ,  $D_3$  and  $D'_3$  in Fig. 2 can be imagined to enclose the incoming and outgoing electromagnetic fields. These subdomains have no further relevance and are not mentioned below. We focus on parts containing the transformation media, which corresponds to  $D'_2$  and  $D_2$  in Fig. 2. To shorten the notation,  $L^{ij}$  is introduced as

$$L^{ij} = \frac{\varepsilon^{ij}}{\varepsilon_0} = \frac{\mu^{ij}}{\mu_0}. \quad (12)$$

We start by describing a device that acts as a two-dimensional analogue of an imperfect electromagnetic wormhole designed using the transformation shown in Fig. 3. The beam enters into the device at one point and leaves it at a distant point almost as if it has passed



a zero optical length while the width of the channel through which the beam goes is small (zero in the ideal case). The device is not invisible (even in the three-dimensional ideal case, the entrances to the wormhole would be visible from the sides) as the one described in [16], but connects distant parts of space. We call it imperfect [24] due to the fact that ideal electromagnetic wormholes require singular material parameters and can be only approximately realized.

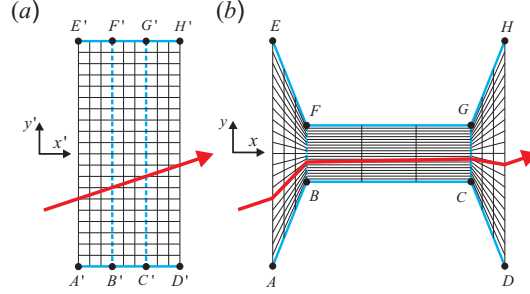


FIG. 3: (Color online) (a) The rectangular electromagnetic domain is mapped onto (b) the polygonal physical domain. A transformation media with material parameters given in (14) for the trapezoid subdomains and (16) for the central rectangular subdomain are required in order to guide the beam along the grid of the physical domain. The red arrow denotes the beam propagation direction corresponding to the simulation in Fig. 6.

According to Fig. 3, two rectangles, the left (L),  $A'B'F'E'$ , and the right one (R),  $C'D'H'G'$ , are gradually narrowed down from  $AE = A'E' = w_0$  to  $BF = w$  and connected by the rectangle between them (the channel) which has been narrowed down to  $w$  and stretched out from  $B'C' = l_0$  to  $BC = l$ . The side rectangles are transformed using

$$x = x' + x_\alpha, \quad y - Y_0 = \Delta_\alpha(y' - Y_0), \quad \Delta_\alpha = a_\alpha x + b_\alpha, \quad \alpha = R, L, \quad (13)$$

while  $z = z'$  in both this and the following examples. The introduced parameters are defined with  $a_L = (w - w_0)w_0^{-1}s^{-1}$ ,  $b_L = 1 - a_L x_A$ ,  $a_R = -a_L$ ,  $b_R = 1 - a_R x_D$ ,  $x_L = 0$ ,  $x_R = l - l_0$ ,  $s = A'B' = C'D' = x_A - x_B = x_C - x_D$ ,  $y = Y_0$  is the symmetry axis of trapezoidal subdomains (in this case  $Y_0 = 0$ ) while  $x_P$  represents the  $x$  coordinate of the point denoted by  $P$ . The material parameters for the left,  $L_L^{ij}$ , and the right,  $L_R^{ij}$ , trapezoids

are found as

$$L_{\alpha}^{ij} = \begin{bmatrix} \Delta_{\alpha}^{-1} & a_{\alpha}\Delta_{\alpha}^{-2}(y - Y_0) & 0 \\ a_{\alpha}\Delta_{\alpha}^{-2}(y - Y_0) & a_{\alpha}^2\Delta_{\alpha}^{-3}(y - Y_0)^2 + \Delta_{\alpha} & 0 \\ 0 & 0 & \Delta_{\alpha}^{-1} \end{bmatrix}. \quad (14)$$

The mapping of the rectangle  $B'C'G'F'$  to the rectangle  $BCGF$  is a simple rescaling

$$x = (x' - x_{B'})\xi + x_B, \quad (y - Y_0) = \gamma(y' - Y_0), \quad (15)$$

where  $\xi = ll_0^{-1}$  and  $\gamma = ww_0^{-1}$  are the stretching and compression parameters. The material parameters for the  $BCGF$  rectangle are

$$L^{ij} = \begin{bmatrix} \xi\gamma^{-1} & 0 & 0 \\ 0 & \xi^{-1}\gamma & 0 \\ 0 & 0 & \xi^{-1}\gamma^{-1} \end{bmatrix}. \quad (16)$$

The beam rotator is a device that rotates the propagation direction of a free-space beam. It is designed using the transformation shown in Fig. 4.

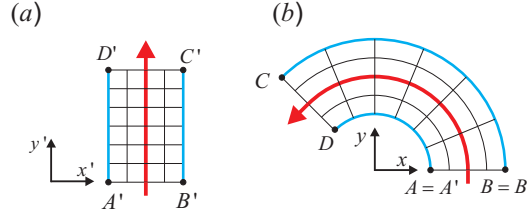


FIG. 4: (Color online) (a) The rectangular electromagnetic domain is mapped onto (b) the annular segment shaped physical domain. A transformation media with material parameters given by (18) needs to be placed in the physical domain to guide the beam along the curved grid. The red arrow shows the beam propagation direction.

The material parameters for a beam rotator are found using the following transformation

$$x = x' \cos(\kappa y'), \quad y = x' \sin(\kappa y'), \quad (17)$$

The rectangle  $A'B'C'D'$  is mapped onto the annular segment  $ABCD$ .  $L = A'D'$  is the optical length that the beam passes going through the device, as indicated by red arrows in Fig. 4. If the device rotates the beam by  $\alpha$ , then  $\kappa L = \alpha$ . Using (3),  $L^{ij}$  is found to be

$$L^{ij} = \begin{bmatrix} \Delta^{-1} \cos^2 \varphi + \Delta \sin^2 \varphi & \sin \varphi \cos \varphi (\Delta^{-1} - \Delta) & 0 \\ \sin \varphi \cos \varphi (\Delta^{-1} - \Delta) & \Delta \cos^2 \varphi + \Delta^{-1} \sin^2 \varphi & 0 \\ 0 & 0 & \Delta^{-1} \end{bmatrix}, \quad (18)$$

where  $\Delta = \kappa\sqrt{x^2 + y^2}$  and  $\varphi = \tan^{-1}(yx^{-1})$ .

More complex geometries are readily implemented by applying several successive transformations. This approach facilitates the design since the material parameters obtained for the first transformation are taken as the initial ones for the second transformation, according to (3). Figure 5 shows a transformation that can be described as a compression followed by a rotation.

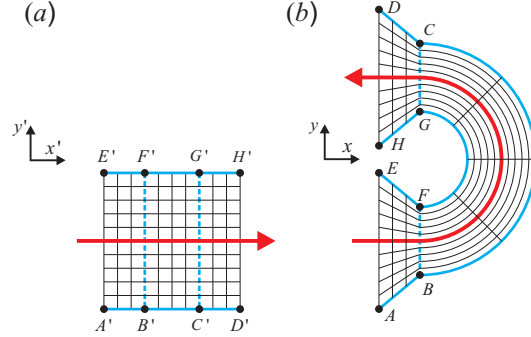


FIG. 5: (Color online) (a) The rectangular electromagnetic domain and (b) the corresponding physical domain. A transformation media with material parameters given in (14) for the trapezoid subdomains and (19) for the curved one needs to be placed to guide the beam along the grid of the physical domain. The red arrow denotes the beam propagation direction.

The rectangle  $B'C'G'F'$  is first compressed and then mapped onto the annular subdomain  $BCGF$ . Using (15) with the parameter of stretching  $\xi = 1$  and (17), the material parameters of the annular subdomain are obtained as

$$L^{ij} = \begin{bmatrix} \Delta_\gamma^{-1} \cos^2 \varphi + \Delta_\gamma \sin^2 \varphi & \sin \varphi \cos \varphi (\Delta_\gamma^{-1} - \Delta_\gamma) & 0 \\ \sin \varphi \cos \varphi (\Delta_\gamma^{-1} - \Delta_\gamma) & \Delta_\gamma \cos^2 \varphi + \Delta_\gamma^{-1} \sin^2 \varphi & 0 \\ 0 & 0 & \Delta_\gamma^{-1} \end{bmatrix}, \quad (19)$$

with  $\Delta_\gamma = \gamma\Delta$ .

The side rectangles, the left (L),  $A'B'F'E'$ , and the right one (R),  $C'D'H'G'$ , are transformed into trapezoids  $ABFE$  and  $CDHG$ , respectively, according to (13), so the material parameters of the trapezoid subdomains are given by (14).

All these devices are two-dimensional because this facilitates their numerical simulation and because a potential implementation, either using metamaterials with the full set of

parameters, or structures with the reduced set of parameters [25], [26], is more likely to be two-dimensional.

In order to confirm the previous considerations, we have performed finite elements (FE) simulations of a beam propagation through the proposed devices using the COMSOL Multiphysics software package. The structures in Figs 6, 7, and 8 are illuminated by transverse electric (electric field is along the  $z$ -axis) monochromatic beams with sources denoted by  $S$ . The computational domains were bounded by PMLs.

The PEC layers on device boundaries were not used in the numerical simulations, as they are irrelevant provided that the fields are negligible on the boundaries. This is fulfilled if the beam width is smaller than the width of the device. In order to meet this condition, the simulations were carried out for the free space wavelength of a beam which provides an acceptable divergence within the devices. Otherwise, the beam would significantly diverge causing reflection on its boundaries and leading to improper work of the device.

Figure 6 shows a beam with oblique incidence passing through the imperfect wormhole. To better illustrate how the fields propagate through the structure, the compression and stretching were chosen to be  $\gamma = 0.15$  and  $\xi = 39$ . The beam is compressed within the left trapezoidal subdomain, it passes through the long channel, and finally, it is expanded to the initial width within the right trapezoidal subdomain. The structure in the electromagnetic domain is twice as wide as the beam, ensuring that the fields do not reach the boundaries. The compression and expanding within trapezoidal subdomains enable a continuous transition from and to the free space. Having passed through the narrow channel, the beam leaves the wormhole translated along the  $x$ -axis retaining its initial propagation direction and field distribution.

The physical implications of geometrical transformations can be described on the example of the channel in Fig. 6. The optical length is the same in the electromagnetic and the physical domain. Since the distances along the  $x$ -axis are  $\xi$  times larger in the physical domain, the phase velocity along the  $x$ -axis inside the channel is  $v_f = \xi c$ , where  $c$  is the phase velocity in the exterior. Particularly, if  $\xi > 1$  and the exterior is vacuum  $v_f$  becomes superluminal emphasizing the dispersion issue in metamaterials that would be used in such devices. Thus stretched structures in vacuum can be realized to work only within a limited bandwidth. In this respect, there is a difference between transformation media that implement a change of topology (such as electromagnetic cloaks [3] or wormholes [16]) and those

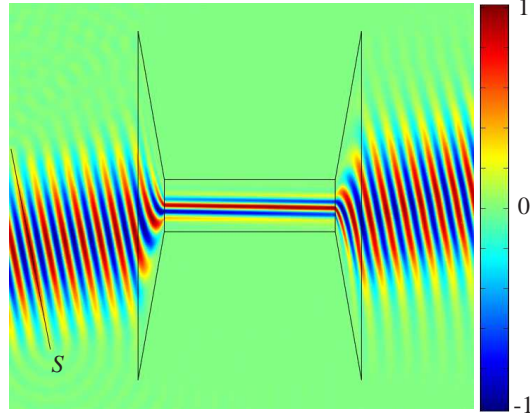


FIG. 6: (Color online) FE simulation results for the distribution of normalized  $z$ -component of electric field,  $E_z(x, y)$ , in presence of the imperfect wormhole. The line denoted by  $S$  is the source of the electromagnetic beam. A structure with  $\gamma = 0.15$  and  $\xi = 39$  was used in the simulation.

that implement a nonsingular geometrical change (field rotators [14] or concentrators [13]). The former employs an infinite stretching around some points and must have parts where  $v_f$  is superluminal independent on the refractive index of the surrounding, while the latter have finite stretching in each point and if immersed in a medium with high enough refractive index may have subluminal  $v_f$  everywhere and not be a priori dispersion limited.

Using (15) and (4) the field intensities in the channel are obtained as

$$H_x = \xi^{-1} H_{x'}, \quad H_y = \gamma^{-1} H_{y'}, \quad E_z = E_{z'}, \quad (20)$$

with  $E_z$  unaltered since two-dimensional transformations leaving the  $z$ -axis invariant are being considered. Equation (20) shows that a rescaling of the geometry is accompanied by a rescaling of the field components. Since the beam propagation direction inside the channel is almost parallel to the  $x$ -axis,  $H_x$  is negligible and  $\xi$  almost has no influence on the fields magnitude in the channel. Hence, in this case the compression determines the increase of the magnetic field intensity in the physical domain.

The field distribution for the beam rotator is shown in Fig. 7. In this example, the propagation direction of the incoming beam is rotated by  $135^\circ$ . The beam width is chosen to be equal to the width of the device. This causes a small degree of scattering on the device boundaries. Nevertheless, the simulation results show that the device still works properly. The beam leaves the rotator unperturbed with the changed propagation direction.

The simulation results for the device designed by applying two successive transformations

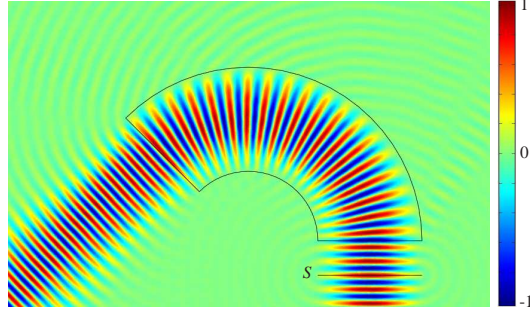


FIG. 7: (Color online) FE simulation results for  $E_z(x, y)$  of the monochromatic beam excited by the source  $S$  and passing through a beam rotator. The angle of rotation is  $135^\circ$ .

are shown in Fig. 8. In the central part of the device, the beam is compressed and rotated. The parameter of compression is  $\gamma = 0.5$  while the angle of rotation is  $180^\circ$ . Therefore, the device focuses the fields within the metamaterial, while the beam leaves it with a reversed propagation direction. As can be seen, the wavelength and the shape of wavefronts are changed within the central part of the device. This corresponds to a linear in  $r$  (the radius of curvature) phase velocity. Arbitrary phase velocities are achieved by choosing the appropriate length of the corresponding part in the electromagnetic domain. Input and output trapezoidal subdomains provide a continuous transition between the free space and the central part of the device and vice versa. The small scattered field around the device is again a consequence of the beam width being equal to the width of the structure. The proper work of the device is proven by undisturbed wavefronts of the rotated beam and the increased beam width in the upper part which is due to the natural divergence of the incoming beam. By choosing wider beams, we have demonstrated the robustness of these devices in situations where the zero-field condition on the boundaries is met only approximately.

In summary, a novel approach to CTM based on confined structures has been described. It relies on explicitly treating the change of boundary conditions when the coordinate transformation is made and the transformation media introduced. We have shown that PEC and PMC boundary conditions remain invariant and used it to explain how orthogonally transformed fields are obtained outside the transformation media. Three detailed examples are given demonstrating the use of approach to design structures that manipulate electromagnetic beams propagating in free space. We have first demonstrated the displacing of a beam along its propagation direction and its rotation by an arbitrary angle.

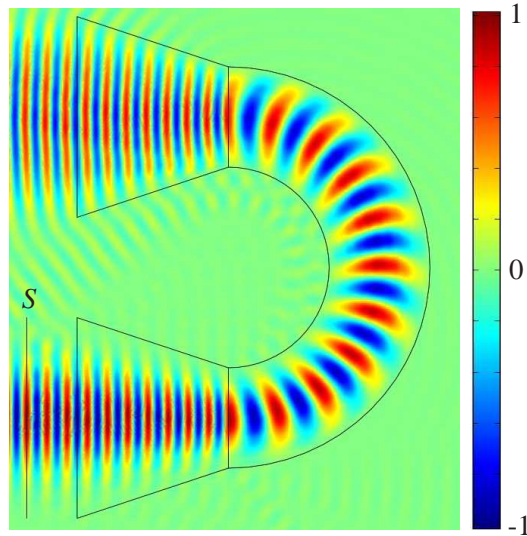


FIG. 8: (Color online) FE simulation results for  $E_z(x, y)$  of the electromagnetic beam excited by the source  $S$  and propagating through an arbitrary complex device. The parameter of compression is  $\gamma = 0.5$  and the angle of rotation is  $180^\circ$ .

### Acknowledgments

This work is supported by the Serbian Ministry of Science project 141047. G. I. acknowledges support from ORSAS in the U. K. and the University of Leeds. R. G. acknowledges support from EU FP7 project Nanocharm. K. H. is grateful for partial support from European Community Project N2T2. We are, also, grateful to Photeon and Heinz Syringer from Photeon Technologies for financial support and Johann Messner from the Linz Supercomputer Center for technical support.

---

\* Electronic address: bvasic@phy.bg.ac.yu

- [1] U. Leonhardt and T. G. Philbin, *New J. Phys.* **8**, 247 (2006).
- [2] J. D. Jackson, *Classical Electrodynamics* (Wiley, New York, 1998).
- [3] J. Pendry, D. Schurig, and D. Smith, *Science* **312**, 1780 (2006).
- [4] D. Schurig, J. B. Pendry, and D. R. Smith, *Opt. Express.* **14**, 9794 (2006).
- [5] J.-P. Berenger, *J. Comput. Phys.* **114**, 185 (1994).
- [6] W. Chew and W. Weedon, *Micro. Opt. Tech. Lett.* **7**, 599 (1994).

- [7] F. Teixeira and W. Chew, IEEE Microwave Guided Wave Lett. **8**, 223 (1998).
- [8] A. J. Ward and J. B. Pendry, J. Mod. Opt. **43**, 773 (1996).
- [9] D. Shyroki, arXiv:physics/0605002v1 [physics.optics] (2006).
- [10] D. M. Shyroki, IEEE Trans. Microwave Theory Tech. **56**, 414 (2008).
- [11] C. Kottke, A. Farjadpour, and S. G. Johnson, Phys. Rev. E **77**, 036611 (2008).
- [12] D. Shyroki, arXiv:physics/0307029v2 [physics.optics] (2007).
- [13] M. Rahm, D. Schurig, D. Roberts, S. Cummer, D. Smith, and J. Pendry, Photonics Nanostruct. Fundam. Appl. **6**, 87 (2008).
- [14] H. Chen and C. T. Chan, Appl. Phys. Lett. **90**, 241105 (2007).
- [15] J. Pendry and S. Ramakrishna, J. Phys.: Condens. Matter **15**, 6345 (2003).
- [16] A. Greenleaf, Y. Kurylev, M. Lassas, and G. Uhlmann, Phys. Rev. Lett. **99**, 183901 (2007).
- [17] M. Rahm, S. A. Cummer, D. Schurig, J. B. Pendry, and D. R. Smith, Phys. Rev. Lett. **100**, 063903 (2008).
- [18] U. Leonhardt and T. G. Philbin, arXiv:0805.4778v2[physics.optics] (2008).
- [19] B. Donderici and F. Teixeira, IEEE Microwave Compon. Lett. **18**, 233 (2008).
- [20] O. Ozgun and M. Kuzuoglu, Microwave Opt. Technol. Lett. **49**, 2386 (2007).
- [21] J. B. Pendry, Phys. Rev. Lett. **85**, 3966 (2000).
- [22] A. Greenleaf, Y. Kurylev, M. Lassas, and G. Uhlmann, Commun. Math. Phys. **281**, 369 (2008).
- [23] O. Ozgun and M. Kuzuoglu, IEEE Microwave Compon. Lett. **17**, 754 (2007).
- [24] G. Isic, R. Gajic, B. Novakovic, Z. V. Popovic, and K. Hingerl, Opt. Express. **16**, 1413 (2008).
- [25] D. Schurig, J. J. Mock, B. J. Justice, S. A. Cummer, J. B. Pendry, A. F. Starr, and D. R. Smith, Science **314**, 977 (2006).
- [26] M. Yan, Z. Ruan, and M. Qiu, Phys. Rev. Lett. **99**, 233901 (2007).